Coarse-graining limits in open and wall-bounded dissipative particle dynamics systems

Igor V. Pivkin and George E. Karniadakis[a)]
Division of Applied Mathematics, Brown University, Providence, Rhode Island 02912

(Received 10 January 2006; accepted 7 March 2006; published online 8 May 2006)

Coarse graining of dense liquid-state systems can potentially lead to fast simulation times, thus providing an effective bridge between atomistic and continuum descriptions. Dissipative particle dynamics (DPD) is a stochastic Lagrangian method that provides a simple formal procedure for coarse graining. Here we analyze some of the fundamental modeling ideas of DPD and identify three factors that limit its application at high coarse-graining levels: interparticle force magnitude, compressibility, and geometric confinement. These artifacts lead to erroneous transport properties of highly coarse-grained DPD systems and thus incorrect dynamics in simulating complex fluids, e.g., colloids and polymers. © *2006 American Institute of Physics*. [DOI: 10.1063/1.2191050]

I. INTRODUCTION

Despite the teraflop speeds of current parallel computer systems, molecular modeling of liquid-state systems based on atomistic simulations is still computationally prohibitive for mesoscopic spatial domains and integration times. To this end, many interesting new methods have been proposed in the last few years focusing on coarse-graining (CG) approaches that yield low-dimensional systems amenable to fast computations in simulation studies of simple and even complex, e.g., biomolecular, liquid systems. Typical CG approaches include the elimination of fast degrees of freedom, clustering of individual atoms into larger single-interaction particles, and spatiotemporal averaging of effective interaction potentials.[1] Other recent CG approaches based on stochastic closures or approximate inertial manifold ideas that could potentially be used for liquid-state systems can be found in Refs. 2 and 3, respectively.

Dissipative particle dynamics[4] (DPD) is a CG method that employs both simplified potentials—that can be thought of as averaged effective potentials[5]—and grouping of atoms into a single particle, i.e., the DPD particle. Specifically, the DPD method describes interacting *clusters* of molecules moving together in a Lagrangian fashion subject to soft repulsive-only potentials. While DPD has been successfully applied in several simulations of complex fluids,[6–9] there are still fundamental unresolved issues that prevent this computationally efficient method from widespread use: they include thermodynamic consistency, coarse-graining artifacts, and anomalous behavior in confined geometries. In the current work, we investigate various aspects of coarse graining and identify the main factors that limit this procedure both in open periodic and in wall-bounded DPD systems. Although we focus our investigation to single-phase liquid systems, our results apply to multiphase complex fluids with significant consequences on the accuracy of their transport dynamics.

[a)]Electronic mail: gk@dam.brown.edu

As a particle-based mesoscopic method, DPD considers N particles, each having mass m_i, whose momenta and position vectors are governed by Newton's equations of motion. For a typical particle i: $\mathbf{v}_i = d\mathbf{r}_i/dt$, and $\mathbf{F}_i = m_i d\mathbf{v}_i/dt$, where $\mathbf{v}_i$ its velocity, $\mathbf{r}_i$ its position, and $\mathbf{F}_i$ its net force. The interparticle force $\mathbf{F}_{ij}$ exerted on particle i by particle j is composed of conservative ($\mathbf{F}_{ij}^C$), dissipative ($\mathbf{F}_{ij}^D$), and random ($\mathbf{F}_{ij}^R$) components. Hence, the total force on particle i is given by $\mathbf{F}_i = \Sigma_{i \neq j} \mathbf{F}_{ij}^C + \mathbf{F}_{ij}^D + \Delta t^{-1/2} \mathbf{F}_{ij}^R$, Δt being the simulation time step. The sum acts over all particles within a cutoff radius r_c beyond which the forces are considered negligible. We set the interaction radius to $r_c = 1$, thus defining the length scale of the system. Denoting $\mathbf{r}_{ij} = \mathbf{r}_i - \mathbf{r}_j$, $\mathbf{v}_{ij} = \mathbf{v}_i - \mathbf{v}_j$, $r_{ij} = |\mathbf{r}_{ij}|$, and the unit vector $\mathbf{e}_{ij} = \mathbf{r}_{ij}/r_{ij}$, the forces are

$$\mathbf{F}_{ij}^C = F^{(C)}(r_{ij})\mathbf{e}_{ij}, \quad \mathbf{F}_{ij}^D = -\gamma \omega^D(r_{ij})(\mathbf{v}_{ij} \cdot \mathbf{e}_{ij})\mathbf{e}_{ij},$$

$$\mathbf{F}_{ij}^R = \sigma_R \omega^R(r_{ij}) \xi_{ij} \mathbf{e}_{ij},$$

where the ξ_{ij} are symmetric Gaussian random variables with zero mean and unit variance and σ_R, γ are coupled by $\sigma_R^2 = 2\gamma k_B T$, k_B being the Boltzmann constant and T the temperature of the system.[10] A common choice for the conservative force is a soft repulsion given by $F^{(C)}(r_{ij}) = a_{ij} \max\{1 - (r_{ij}/r_c), 0\}$. The dissipative and random forces, on the other hand, are characterized by strengths $\omega^D(r_{ij})$ and $\omega^R(r_{ij})$ coupled by $\omega^D(r_{ij}) = [\omega^R(r_{ij})]^2 = \max\{(1 - (r_{ij}/r_c))^2, 0\}$. The above relation is necessary for thermodynamic equilibrium.[10] The pair of dissipative and random forces constitutes the DPD local thermostat. We will refer to this method as the DPD-Verlet version as we will employ a modified Verlet algorithm to integrate the stochastic equations of motion.[11]

An alternative DPD method that employs the Andersen thermostat, instead of the aforementioned pair of forces, has been proposed by Lowe.[12] This method achieves realistic values of the Schmidt number and is less sensitive to the size of the integration time step. Thermal equilibrium is achieved probabilistically by drawing relative velocities from a Maxwell distribution, just like in molecular dynamics (MD)

simulations, but for pairs of particles within r_c instead of individual particles as in MD. The probability is $0 \leqslant \Gamma \Delta t \leqslant 1$, where Γ is the thermalization parameter with large values corresponding to thermalization of almost all particles. In general, the DPD-Lowe fluid is very viscous so it is of interest to investigate both the DPD-Verlet and the DPD-Lowe versions.

The computational advantage of DPD compared to MD for mesoscopic systems stems from the use of soft potentials as well as the clustering of N_m atoms into a large DPD particle. Experience with DPD simulations and scaling arguments (see Ref. 7) shows that the combined computational speedup, say, for water simulation, is about $1000N_m^{5/3}$, which for $N_m=5$ and 10 gives the large factors of 73 000 and 464 000, respectively. Clearly, such accelerated simulations, especially at $N_m \geqslant 10$, allow for laptop-based mesoscopic simulations of complex biomolecular systems where water is the main component. The question, however, we address in this work is what are the fundamental and practical factors that limit large values of N_m, and what kind of "fingerprint" monitoring is required to be developed in order to recognize the potential limits and associated numerical artifacts.

In the following, we present first the DPD CG procedure in Sec. II, and in Secs. III and IV we deal separately with open (periodic) and wall-bounded DPD systems, respectively. In Sec. V we investigate the effect of different parameters in the DPD and Andersen thermostats on the N_m limits that we obtained in the previous sections. We conclude in Sec. VI with a brief summary and a discussion on how the observed artifacts affect adversely the dynamics of complex fluids, e.g., polymers and colloids.

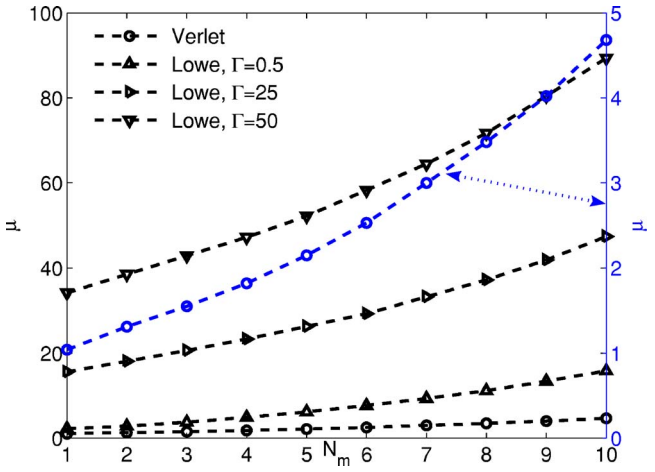

FIG. 1. (Color online) Dynamic viscosity (DPD units) of the DPD fluid as a function of N_m. The dashed line in the DPD-Verlet fluid (circles) is a second-order polynomial fit. The right vertical axis corresponds to the Verlet viscosity only.

$$M = mN_m, \tag{1}$$

$$r_c = \left(\frac{N_m \rho^*_{\mathrm{DPD}}}{\rho_{\mathrm{MD}}} \right)^{1/3} \sigma, \tag{2}$$

$$a = k_B T \frac{\kappa^{-1} N_m - 1}{2\alpha \rho_{\mathrm{DPD}}}, \tag{3}$$

$$\tau_{\mathrm{DPD}} = \frac{\nu^*_{\mathrm{DPD}}}{\nu_{\mathrm{MD}}} \left(\frac{r_c}{\sigma} \right)^2 \tau. \tag{4}$$

II. DPD COARSE-GRAINING PROCEDURE

We will apply coarse graining to a Lennard-Jones (LJ) fluid of density $\rho_{\mathrm{MD}}=0.8\sigma^{-3}$ in a domain $34.2\sigma \times 8.55\sigma \times 34.2\sigma$ in x-y-z, where σ is the atomic diameter. The viscosity of the LJ fluid was obtained via nonequilibrium MD simulations using Lees-Edwards boundary conditions and is equal to $1.97m/(\sigma\tau)$, where m and τ are MD units of mass and time, correspondingly. The dimensionless compressibility $\kappa^{-1}=15.36$ was found by conducting equilibrium isothermal MD simulations, where the pressure was computed over a range of densities, for details we refer to Ref. 13.

The degree of coarse graining in DPD is characterized by the number N_m of LJ atoms contained in a DPD particle. Thus, the mass M of a DPD particle is N_m times the mass of a MD particle, and we also set the DPD fluid density ρ_{DPD} equal to $3r_c^{-3}$. The cut-off radius r_c can be found by equating the mass densities of the MD and DPD systems while the DPD time scale can be related to the MD time scale by setting the shear viscosities of the corresponding fluids to be the same. The conservative forces present in the DPD equations $F^{(C)}(r_{ij})$ are associated with the equation of state of the DPD fluid (see Ref. 11) since the magnitude $a=a_{ij}$ of the conservative force is determined by the dimensionless compressibility κ^{-1}. The main equations are summarized below: The variables marked with the symbol * have the same numerical values as in DPD but they have units of MD. The coefficient α in Eq. (3) was determined to be $\alpha=0.101\pm0.001$ in Ref. 11. The DPD simulation parameters can be expressed in reduced MD units using these equations.

We first compute the viscosity of DPD fluid for $k_BT=0.1$ $(\sigma_R=3, \gamma=45)$ and different values of the coarse-graining parameter N_m based on the Lees-Edwards method.[14] In Fig. 1 we plot representative values of the dynamic viscosity μ for both the DPD-Verlet and the DPD-Lowe methods. We note that even for small values of the thermalization parameter Γ the DPD-Lowe fluid is more viscous than the DPD-Verlet fluid. In the latter case for $N_m \leqslant 10$ the viscosity increases approximately as N_m^2.

In the coarse-graining procedure we keep the DPD density constant as we need to have $\rho_{\mathrm{DPD}} \geqslant 3r_c^{-3}$ in order to have a liquid phase;[11] hence, the volume of the domain has to decrease accordingly as we increase N_m. In Table I we present the domain size for different values of N_m.

TABLE I. Size of the domain in DPD units at different coarsening levels.

N_m	1	5	9	13	17
L	22.01	12.87	10.58	9.36	8.56

III. OPEN DPD SYSTEMS

We first investigate the effect of coarse graining by performing DPD-Verlet simulations in a fully periodic domain of size $(10r_c)^3$ containing 3000 particles. The temperature of the fluid is set to $k_BT=0.1$ and the DPD force parameters are $\sigma_R=3$ and $\gamma=45$. [Equation (3) is used to calculate the conservative force parameter a.] The modified velocity Verlet method (with $\lambda=0.5$) (Ref. 11) and a time step of 0.02 are used to advance the system in time. Initially, all DPD particles are densely packed occupying only a small fraction of the computational domain. After letting the fluid to equilibrate for 80 000 time steps, we record the mean-square displacement (MSD) for 20 000 steps.

In three dimensions and for periodic equilibrium systems, the MSD of atoms is related to the diffusion coefficient D through the Einstein relation

$$D = \lim_{t\to\infty} \frac{\langle [\mathbf{r}(t) - \mathbf{r}(0)]^2 \rangle}{6t}. \tag{5}$$

Equation (5) implies that for large times the mean-square displacement grows linearly. The diffusion coefficient is obtained by calculating the slope of MSD versus time in the asymptotic regime. (For nonequilibrium systems the displacement of the atoms due to the bulk transport is subtracted.) In Fig. 2 we plot the MSD for the $N_m=1$ and $N_m=100$ cases. The former shows the initial quadratic response and the subsequent linear growth with time, as expected; however, in the latter ($N_m=100$) we observe a very different behavior, more characteristic of *solidlike* structures. In Fig. 2 we plot the diffusion coefficient D computed for different levels of coarse graining of the DPD fluid. The values of D gradually decrease with N_m, and for $N_m=30$ the diffusion coefficient is about 450 times smaller than that for $N_m=1$.

For homogeneous substances the structural arrangement of atoms depends only on the distance r between atoms. The radial distribution function (RDF) is proportional to the probability of finding two atoms separated by distance r and it is defined by

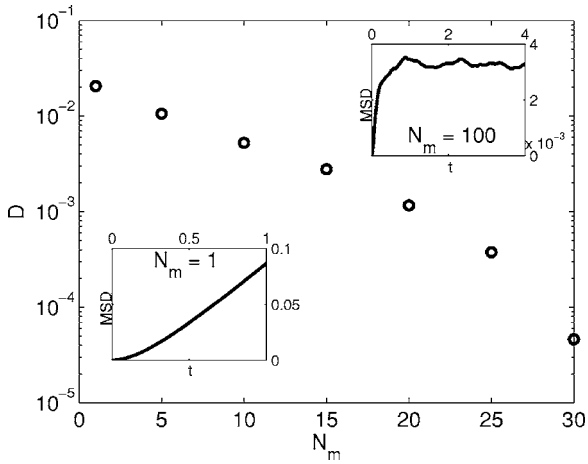

FIG. 2. Diffusion coefficient as a function of the coarsening parameter N_m and mean-square displacements for $N_m=1$ and $N_m=100$ measured in a large periodic domain. (The results are shown in DPD units.)

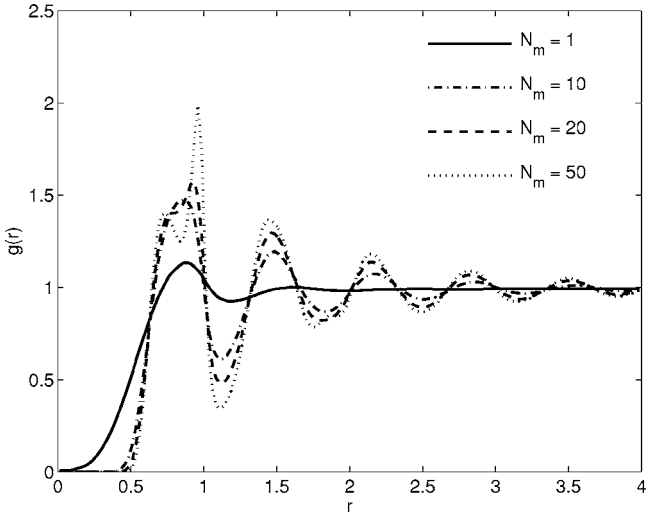

FIG. 3. Radial distribution function for different N_m in an open DPD system (DPD units).

$$g(r) = \frac{1}{N\rho_{\mathrm{DPD}}} \left\langle \sum_i^N \sum_{i\neq j}^N \delta[r - r_{ij}] \right\rangle. \tag{6}$$

Here, N is the total number of atoms, ρ_{DPD} is the number density, r_{ij} is the distance between centers of atoms i and j, and the angular brackets represent time averaging. In Fig. 3 we present the radial distribution functions for different levels of coarse graining N_m. In all cases $g(r)$ is computed using equilibrium simulations with 3000 particles in the fully periodic domain of size $(10r_c)^3$. The simulations were run for 12 000 time steps and the RDF was computed during the last 2000 steps. RDF is a helpful indicator of the nature of the phase assumed by the simulated system.[15] For atoms frozen onto the sites of regular lattice structures, $g(r)$ takes the form of a sequence of *delta* distributions whereas for gases $g(r) \equiv 1$. If atoms are vibrating about rather than being fixed to the lattice sites, then the delta distributions in $g(r)$ resolve into Gaussians. For partially crystallized substances, $g(r)$ may contain secondary peaks not found in $g(r)$ for a liquid. Such additional peaks are caused by remnants of the lattice structure and can be readily seen in Fig. 3 for $N_m \geqslant 20$.

Next we study the effect of coarse graining on the speed of sound in the DPD fluid as this will provide an estimate of compressibility in the coarse-grained DPD system. The isothermal speed of sound is given by

$$c = \sqrt{k_BT + \frac{4\pi\rho}{3} \int_0^\infty |F^C(r)| g(r) r^3 dr} \tag{7}$$

and can be obtained from the DPD equation of state[11]

$$p = \rho k_BT + \frac{2\pi\rho^2}{3} \int_0^\infty |F^C(r)| g(r) r^3 dr, \tag{8}$$

where $|F^C(r)|$ is the magnitude of the conservative force. The values of the speed of sound given by Eq. (7) as a function of N_m are plotted in Fig. 4. We note here that c increases approximately as $N_m^{1/2}$.

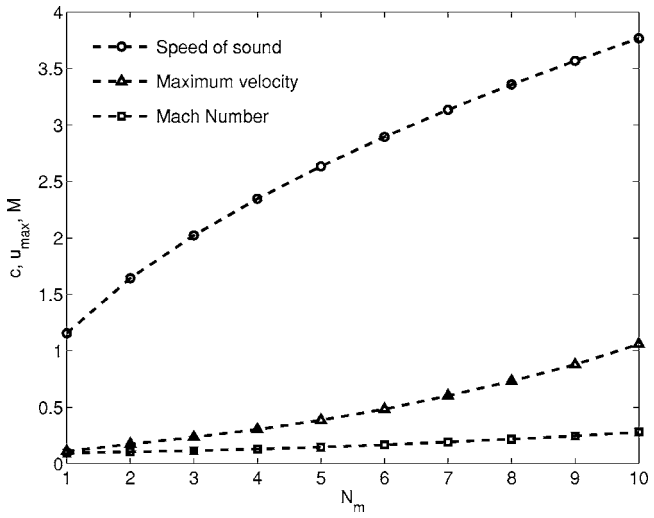

FIG. 4. Speed of sound c, Poiseuille flow maximum velocity $u_{\max}$ (DPD units), and Mach number M as functions of N_m.

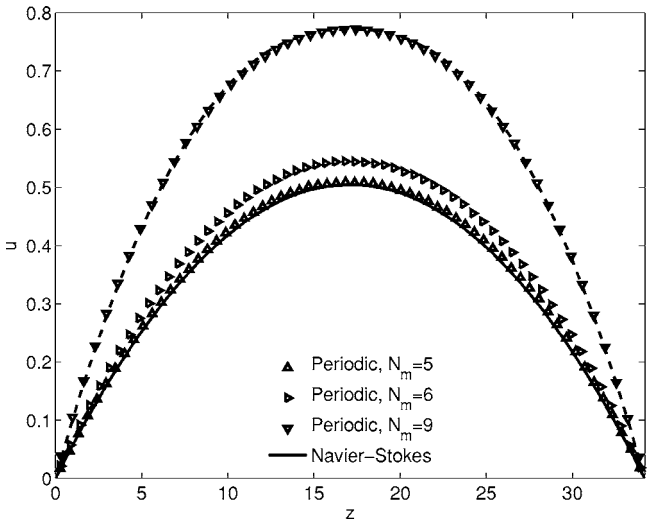

FIG. 5. Velocity profiles in Poiseuille flow obtained using the periodic boundary condition for different levels of coarse graining. (The results are shown in MD units.)

In summary, in this section we have shown that for the specific periodic system we have examined there seems to be an artificial solidification taking place for $N_m \geqslant 20$ at $k_BT=0.1$. It is also in agreement with the findings of Ref. 16 where such solidification was reported for values of the conservative force coefficient $a \geqslant 250$ for temperature level $k_BT=1$. Using Eq. (3) we find that the corresponding value of the coarsening parameter is $N_m \geqslant 10$, which is more conservative than the limit we established *directly* here.

IV. WALL-BOUNDED DPD SYSTEMS

We now turn our attention to confined DPD fluid flows. In particular, we will examine Poiseuille flow with two different models for the effect of the wall: (a) ideal periodic walls and (b) solid DPD walls. We will investigate for both cases the effect of the coarse graining by examining similar quantities as in the previous section.

In the first boundary condition model, we set up two adjacent counterflowing Poiseuille flows using periodic boundaries.[17] Specifically, a rectangular domain is doubled in size in the cross flow z direction and the flow is sustained by applying a body force (x direction) to each particle; the direction of the force is opposite in the two halves of the domains. This periodic Poiseuille flow method (PPFM) produces a flow with uniform density from wall to wall apart from the statistical fluctuations. The absence of density artifacts makes PPFM useful for studying the bulk Poiseuille flow (in the continuum limit), i.e., without any density oscillations associated with the presence of solid boundaries. In the second boundary condition type, we model the walls using layers of frozen DPD particles in combination with bounce-back reflections.[18] Specifically, the solid walls are modeled by layers of equally spaced particles and the density of the walls is equal to that of the fluid. To prevent the penetration of fluid particles into the solid regions, bounce-back reflections are applied at the fluid-solid interface. The method is based on an *equivalent force* between wall particles and DPD particles to impose the no-slip condition. The conservative force coefficient of the fluid-solid interactions is adjusted to achieve no-slip conditions at the walls and desired density level in the middle of the channel.[18]

We report first results with the ideal walls. We employ the same domain as described in Sec. II and we double it in the z direction while a body force $F=0.0085m\sigma/\tau^2$ is applied in the x direction. The simulations are carried out for 410 000 time steps using the Verlet algorithm while the flow data are collected over the last 40 000 steps by subdividing the z direction into bins of size $0.2r_c$. These results are further averaged over both halves of the domain.

Streamwise velocity profiles for representative values of the coarsening parameter N_m are shown in Fig. 5. The agreement with incompressible Navier-Stokes solution for Poiseuille flow is good for $N_m \leqslant 5$. For $N_m=6$ there is a slight deviation of the computed velocity profile from the analytic prediction as well as an increase of the temperature inside the domain (not shown here). For higher N_m, the results differ significantly from the incompressible Navier-Stokes solution. In particular, for the velocity profile shown in the figure corresponding to $N_m=9$ we fitted a typical non-Newtonian velocity profile of the form $u_{\max}[1-(|L-z|/L/2)^{1/n+1}]$ and obtained $n=0.738<1$, typical of polymer solutions.

To understand these results, we consider the scaling of DPD units of the body force with N_m using an approximate analysis. Let us ignore, at first, the dependence of the DPD length scale on the coarse-graining parameter N_m. As noted in Sec. II the viscosity of the DPD fluid increases approximately as N_m^2. Since the DPD time scale is roughly proportional to the DPD viscosity, we see that, as a first approximation, the DPD unit of force scales as N_m^4. Assuming the validity of the incompressible Poiseuille flow solution, we obtain that the velocity $u_{\max}$ at the center of the channel scales approximately as N_m^2. Given that the speed of sound is roughly only proportional to $N_m^{1/2}$, we obtain that the Mach number scales as $N_m^{3/2}$, thus increasing with N_m. In Fig. 4 we plot the velocity $u_{\max}$ and the Mach number $M=u_{\max}/c$ computed without ignoring the dependence of the DPD unit of length r_c on N_m; the computed results are consistent with the

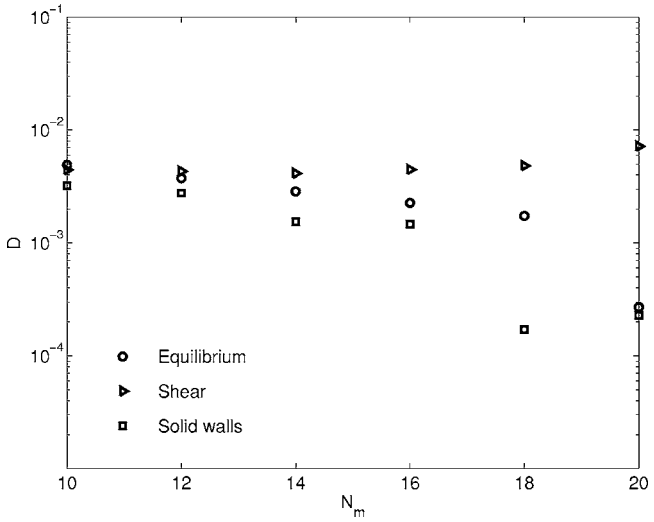

FIG. 6. Diffusion coefficient (DPD units) for different N_m measured in a small domain with periodic walls (shear) and with solid walls in Poiseuille flow. For comparison the diffusion coefficient at zero flow (equilibrium) in a corresponding periodic domain is also shown.

approximate analysis. Specifically, for $N_m > 5$ the Mach number is greater than 0.15 and hence compressibility effects start becoming important.

In order to document this point more accurately we also examine the influence of the domain size in the spanwise y direction which becomes relatively small for high N_m (see Table I). To this end, we first repeat the simulations in a larger domain by increasing the spanwise dimension by four times, i.e., from 8.55σ to 34.2σ. The results are essentially the same as in the small domain, and therefore we eliminate the spanwise size of the domain as a reason for the deviation of simulation results for large N_m from the incompressible Poiseuille flow solution. Next, we repeat the simulations with the body force *decreased* by 90%, i.e., $F = 0.000\,85 m\sigma/\tau^2$. In this case the predicted Mach number is less than 0.15 (up to $N_m \leqslant 20$) and the simulation results are in agreement with the incompressible Poiseuille flow for $N_m \leqslant 10$, that is, we almost double the limit above which deviations occur by suppressing compressibility effects. This illustrates one of the limits of the coarse-graining procedure: due to the specific scaling of the DPD units for large values of N_m the Mach number may become large and, hence, compressibility effects cause deviations from the incompressible continuum solutions.

We further coarse grain the system keeping the body force small so that the Mach number is kept less than 0.15 in the considered range of N_m values. For $N_m > 10$, in both the small and enlarged domains, large increases in temperature and relatively small deviations from the parabolic velocity profile are observed. These effects are likely caused by partial solidification of the DPD system even though the diffusion coefficient remains approximately constant as a result of shearing (see Fig. 6) in contrast to the open system; no specific crystal structure is observed as we coarse grain the system for $N_m \leqslant 20$.

As we have already seen for open systems, the DPD fluid solidifies at high levels of coarse graining as a result of

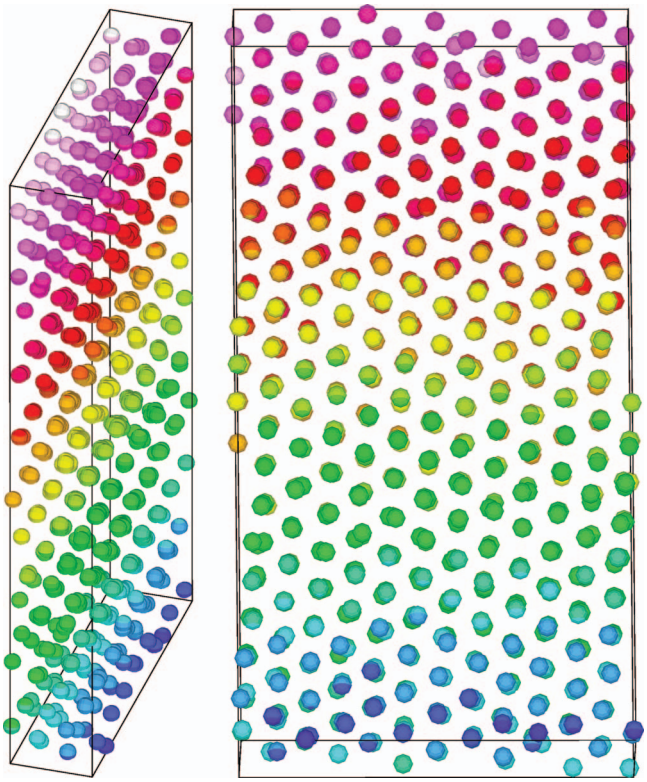

FIG. 7. (Color) Crystal structure formed in a small periodic domain for $N_m = 20$. A simple cubic (sc) lattice structure is observed for this case.

relatively large magnitude of the conservative force. In addition, the DPD unit of length r_c is proportional to $N_m^{1/3}$, i.e., it increases with N_m. Correspondingly, the size of the computational domain in DPD units decreases, as shown in Table I, in order to maintain constant density. Such a geometric constraint may affect the results when shear is imposed through the aforementioned PPFM approach or by explicitly imposing the wall no-slip condition. In the absence of the body force, i.e., in equilibrium simulations in the small *periodic* domain, the system behavior also changes with N_m. In Fig. 6 we plot the computed diffusion coefficient D for $N_m \leqslant 20$. There is a sudden drop of D at $N_m = 20$ due to formation of a crystal structure inside the domain. The crystal structure shown in Fig. 7 formed after a long-term time integration, i.e., approximately 200 000 simulation steps.

Now we report results based on DPD simulations with the second type of boundary conditions, i.e., the solid walls, which tend to induce density fluctuations close to the wall. These fluctuations become larger when the conservative force parameter a increases as we coarse grain the system. In Ref. 13 it was found that density fluctuations can affect the simulation results for N_m as low as 5. The solid-wall induced layering of DPD particles close to the walls is observed as we coarse grain the system starting from low levels of N_m. This facilitates the structuring of the DPD fluid and in equilibrium simulations, similar to the aforementioned ones, crystallization occurs at $N_m = 18$. The dependence of the diffusion coefficient D on N_m is presented in Fig. 6; we observe a sudden drop in D at $N_m = 18$ for this case.

V. EFFECT OF THERMOSTATS

So far we have examined effects of coarse graining due to the conservative coefficient, the Mach number, and the geometric confinement. Next, we discuss how these results change if the basic DPD thermostat, consisting of the pair of dissipative and random forces, changes. We also obtain results with the alternative DPD-Lowe method.

First, we investigate the effects of random force coefficient σ_R on the DPD coarse-graining limits. To this end, we perform equilibrium simulations in a fully periodic domain of size $(10r_c)^3$ with $N_m=20$ and $\sigma_R=3,5,7$. (For $\sigma_R=5$ and 7 the time step is decreased from 0.02 to 0.01 and 0.005, respectively, to achieve stable simulations with temperature $k_BT=0.1$.) We found that the computed RDFs are almost identical, thus the choice of σ_R does not seem to affect the structure of the DPD fluid. Similarly, the speed of sound remains constant as σ_R varies; also the volume of the domain, and thus the geometric confinement, is independent of σ_R.

In order to also consider the effect of temperature on the DPD fluid structure, we performed simulations at different temperature levels in the same fully periodic domain of size $(10r_c)^3$. A DPD fluid was simulated with $N_m=20$. The simulations were repeated with fixed $\sigma_R=3$ and $\gamma=450$, 45, and 4.5 with corresponding temperature levels at $k_BT=0.01$, 0.1, and 1.0, respectively. (In the simulations with $k_BT=0.01$ the time step is decreased to 0.002.) We found that the computed RDFs are unaffected by the temperature chosen in the considered range.

Finally, we considered the DPD-Lowe[12] method with the alternative Andersen-type thermostat that can be tuned by employing different values of the thermalization parameter Γ. Equilibrium simulations were carried out in a periodic domain of size $(10r_c)^3$ at $k_BT=0.1$. The time step was set to 0.02 in DPD units and the system was simulated for 12 000 time steps with the statistics collected over the last 2 000 steps. We simulated two extreme cases where the percent of DPD particles being thermalized at each time step are 1% and 100% for $\Gamma=0.5$ and 50, respectively. Here too, we observed that the computed RDFs for different levels of coarse graining are the same for both values of Γ and are almost identical to those obtained from the aforementioned DPD-Verlet method simulations. This suggests that the structure of the DPD fluid simulated with the Andersen thermostat is the same to the one obtained with the standard DPD thermostat. Therefore, we expect both fluids to solidify at the same level of coarse graining in equilibrium conditions, which is indeed the case as we have verified with DPD-Lowe simulations.

There is a significant difference, however, of the DPD-Lowe method with the standard DPD-Verlet method in nonequilibrium simulations as the former yields fluids with much larger viscosity. We computed the dynamic viscosity using the periodic Poiseuille flow method.[17] Three values of Γ were used in the simulations, $\Gamma=0.5$, 25, and 50. The calculated values of the dynamic viscosity for different N_m are plotted in Fig. 1 along with the DPD-Verlet fluid viscosity.

We note that the dynamic viscosity in all cases is higher than the one in DPD-Verlet simulations. Therefore, the DPD unit of force is expected to be larger in Lowe than in Verlet simulations. Consequently, the predicted Mach numbers for all levels of coarse graining of the Poiseuille system are in the supersonic regime for $\Gamma=25$ and 50! Thus, for Γ between 0.5 and 50 compressibility effects are expected to be significantly more pronounced with the DPD-Lowe thermostat than with the DPD-Verlet thermostat. Finally, we note that the DPD unit of length does not depend on the choice of thermostat and therefore the geometric constraints in simulations are the same for both methods.

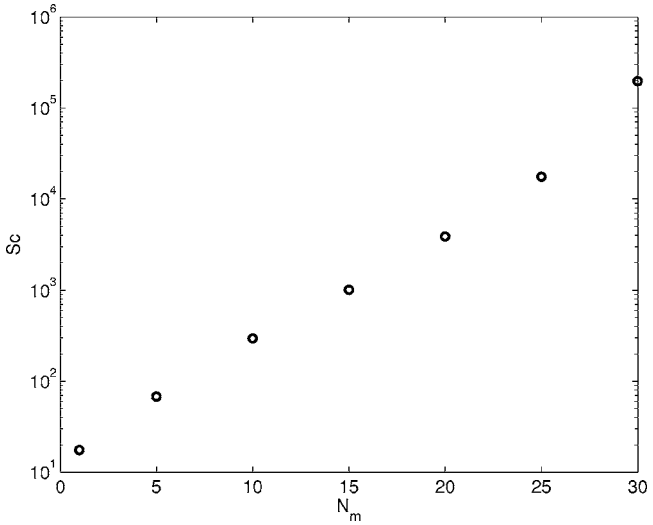

FIG. 8. Schmidt number as a function of the coarsening parameter N_m for DPD-Verlet fluid in a large periodic domain.

VI. SUMMARY AND DISCUSSION

We have considered liquid-state systems both in equilibrium and in Poiseuille flow in order to investigate the fluid states as a function of the coarse-graining parameter N_m that expresses how many atoms are packed in a DPD particle. So far the majority of published work has considered $N_m=1$ in applications although the original developers of DPD advocated coarse-grained versions with $N_m>1$, see Refs. 4, 10, and 11. In the current work we identified fundamental and practical limits of coarse graining in DPD due to the following three factors. (1) Solidification of the DPD liquid due to the increase in the magnitude of the conservative force. (2) Compressibility effects due to the increase of the Mach number in nonequilibrium simulations. (3) Geometry constraints due to the decrease of size of the computational domain. The minimum value of N_m set by these limits determines the maximum level of coarse graining and it depends on the particular system being simulated. In addition, we investigated the effects of thermostats and observed that the fluid structure remains basically the same irrespective of the thermostat, i.e., artificial crystallization is often observed above $N_m>20$.

A modified version of DPD considers local multibody interactions (M-DPD) in order to restore thermodynamic consistency in the method.[19] For equilibrium systems it has been shown that M-DPD can extend the upper limit of N_m by

about an order of magnitude.[16] Also, a Voronoi-based lattice version of DPD (Ref. 20) does not suffer from the aforementioned artifacts, however, it requires the construction of the Voronoi diagram in three dimensions at every time step which is tedious and computationally very intensive. We also note that the artifacts reported in the current work are different than the well-known artifacts attributed to large time steps in the DPD simulations as has been reported in previous works, e.g., see Ref. 21.

While we have focused our analysis on single-phase liquid systems, it is clear that the observed artifacts have significant adverse consequences on the dynamics of complex fluids (e.g., polymers and colloids) or other multiphase systems. This is evident by considering the Schmidt number of one of the systems we have already studied, e.g., the open large system (results are plotted in Figs. 1 and 2). In Fig. 8 we have plotted the corresponding Schmidt number as a function of the coarse-graining parameter N_m, computed based on the viscosity and diffusivity values in Figs. 1 and 2, respectively. We see that the Schmidt number values change by at least *five orders* of magnitude and, in fact, they tend to infinity for larger values of N_m (see Fig. 2). This, in turn, will affect dramatically the polymer dynamics as we have observed in simulations of DNA in microchannels,[22] where both the depletion layer and the mean extension are very sensitive to Schmidt number.

ACKNOWLEDGMENTS

This research is funded by the National Science Foundation Grant No. 506312 under the IMAG program for Multiscale Modeling. Computations were performed at University of Illinois/NCSA, Pittsburgh Supercomputing Center/PSC, and University of California/NPACI facilities.

[1] S. Izvekov and G. A. Voth, J. Chem. Phys. **123**, 134105 (2005).
[2] M. A. Katsoulakis, A. J. Majda, and D. G. Vlachos, Proc. Natl. Acad. Sci. U.S.A. **100**, 782 (2003).
[3] C. Theodoropoulos, Y.-H. Qian, and I. G. Kevrekidis, Proc. Natl. Acad. Sci. U.S.A. **97**, 9840 (2000).
[4] P. J. Hoogerburgge and J. M. Koelman, Europhys. Lett. **19**, 155 (1992).
[5] B. M. Forrest and U. W. Suter, J. Chem. Phys. **102**, 7256 (1995).
[6] N. A. Spenley, Europhys. Lett. **49**, 534 (2000).
[7] R. D. Groot and K. L. Rabone, Biophys. J. **81**, 725 (2001).
[8] A. Maiti and S. McGrother, J. Chem. Phys. **120**, 1594 (2004).
[9] N. S. Martys, J. Rheol. **49**, 401 (2005).
[10] P. Espanol and P. Warren, Europhys. Lett. **30**, 191 (1995).
[11] R. D. Groot and P. B. Warren, J. Chem. Phys. **107**, 4423 (1997).
[12] C. P. Lowe, Europhys. Lett. **47**, 145 (1999).
[13] E. E. Keaveny, I. V. Pivkin, M. Maxey, and G. E. Karniadakis, J. Chem. Phys. **123**, 104107 (2005).
[14] A. W. Lees and S. F. Edwards, J. Phys. C **5**, 1921 (1972).
[15] J. M. Haile, *Molecular Dynamics Simulation: Elementary Methods* (Wiley, New York, 1992).
[16] S. Y. Trofimov, Ph.D. thesis, Eindhoven University of Technology, 2003.
[17] J. A. Backer, C. P. Lowe, H. C. J. Hoefsloot, and P. D. Iedema, J. Chem. Phys. **122**, 154503 (2005).
[18] I. V. Pivkin and G. E. Karniadakis, J. Comput. Phys. **207**, 114 (2005).
[19] I. Pagonabarraga and D. Frenkel, Mol. Simul. **25**, 167 (2000).
[20] M. Serrano, G. de Fabritiis, P. Espanol, E. G. Flekkoy, and P. V. Coveney, J. Phys. A **35**, 1605 (2002).
[21] A. F. Jacobsen, O. Mouritsen, and G. Besold, J. Chem. Phys. **122**, 204901 (2005).
[22] V. Symeonidis, Ph.D. thesis, Brown University, 2005.